

Signatures of orbital selective Mott state in doped  $\text{Sr}_3\text{Ru}_2\text{O}_7$ Buddhadeb Debnath <sup>1</sup>, Anirban Das,<sup>1,2</sup> Priyo Adhikary <sup>1,2</sup> and Shantanu Mukherjee<sup>1,2,3</sup><sup>1</sup>*Department of Physics, Indian Institute of Technology Madras, Chennai 600036, Tamil Nadu, India*<sup>2</sup>*Center for Atomistic Modelling and Materials Design, IIT Madras, Chennai 600036, Tamil Nadu, India*<sup>3</sup>*Quantum Centres in Diamond and Emergent Materials (QCenDiem)-Group, IIT Madras, Chennai 600036, Tamil Nadu, India*

(Received 5 September 2022; accepted 9 March 2023; published 22 March 2023)

Bilayer Strontium Ruthenate  $\text{Sr}_3\text{Ru}_2\text{O}_7$  is a strongly correlated electronic system that shows diverse electronic and structural phases. Upon doping with Mn, an orbital selective Mott phase is observed before the material transitions to a Mott insulating state. Additionally, Mn doping leads to the emergence of an antiferromagnetic state with  $\mathbf{q}_{AFM} = (\pi/2, \pi/2)$  ordering wave vector. Quasiparticle interference (QPI) experiments find a sharp but highly dispersive peak at the AFM wave vector. Another set of QPI peaks is observed at  $\mathbf{q}^* = (\pi, 0)$ , possibly due to a charge order effect. In this work we utilize a tight binding model relevant to Mn doped  $\text{Sr}_3\text{Ru}_2\text{O}_7$ , and show that the origin of observed orbital selective Mott phase is inherently dependent upon the presence of a strong onsite exchange interaction and oxygen octahedral rotation suppression induced by the Mn doping. We further find that the experimentally observed QPI spectra, including the peaks at  $\mathbf{q}_{AFM}$ , and  $\mathbf{q}^*$  wave vectors can be concomitantly explained within this formalism.

DOI: [10.1103/PhysRevMaterials.7.035001](https://doi.org/10.1103/PhysRevMaterials.7.035001)

## I. INTRODUCTION

Strongly correlated metals often show a bad metal behavior where the renormalized Landau quasiparticles are associated with electronic transport properties. For materials with multiple low energy bands, the orbital resolved quasiparticle renormalizations can selectively make certain orbitals incoherent leading to an orbital selective Mott phase (OSMP) [1–6]. However, the formation of an OSMP is not ubiquitous and depends intricately upon the strength of Hund's rule coupling [7,8] and crystal field effects [9] that lead to a broken orbital degeneracy. A strong interorbital interaction further helps stabilize an orbital selective state by suppressing orbital fluctuations [7]. A number of recent studies show that orbital selectivity can play an important role in the formation of novel low temperature phases of quantum materials including magnetism [10–12], charge ordering [13], nematic ordering [14], and superconductivity [15,16].

The bilayer compound  $\text{Sr}_3\text{Ru}_2\text{O}_7$  has generated significant interest due to the complex interplay between its various ordered phases [17–21]. It is a strongly correlated  $4d$  orbital material [22] that undergoes a metamagnetic transition in the presence of an external magnetic field [18]. When doped with Mn,  $\text{Sr}_3(\text{Ru}_{1-x}\text{Mn}_x)_2\text{O}_7$  undergoes a transition to a long range antiferromagnetic order [23–25] and a metal insulator transition [3,26] for  $x > 0.05$ . Although the origin for the metal insulator transition has been debated [27], a number of studies [8,26,27] suggest that the insulator is likely to be an electronic correlation driven Mott insulator. An important property present in the bilayer compound  $\text{Sr}_3\text{Ru}_2\text{O}_7$  is the presence of an effective rotation of around  $\sim 6^\circ$  in the oxygen octahedra surrounding the Ru ions leading to a doubling of the unit cell [24,28]. It has been observed that the rotation angle is continuously suppressed with Mn doping [24], and the corresponding effect on the electronic structure supports

the formation of antiferromagnetic order [24,25,29] and a low temperature Mott insulating phase [3,26].

Recent angle resolved photo emission spectroscopy (ARPES) experiments on  $\text{Sr}_3\text{Ru}_2\text{O}_7$  find that the doping induced Mott insulating phase is preceded by a metallic phase where the  $d^{xy}$  orbital dominated  $\gamma$  Fermi pocket vanishes at around 5% Mn doping at low temperatures [3]. This behavior has been ascribed to an orbital selective Mott transition where the  $d^{xy}$  orbital quasiparticle weight ( $Z_{xy} < Z_{yz/xz}$ ) is strongly suppressed. The origin of the orbital selectivity in Mn doped  $\text{Sr}_3\text{Ru}_2\text{O}_7$  currently remains unexplored. Although strong correlation studies in Mn doped  $\text{Sr}_3\text{Ru}_2\text{O}_7$  are lacking, previous theoretical studies of correlation effects in undoped  $\text{Sr}_3\text{Ru}_2\text{O}_7$  [30] utilize a density functional theory (DFT) + rotationally invariant slave boson mean field theory find the quasiparticle weights to be weakly orbital selective, with an opposite behavior to experimental observation in doped compound ( $Z_{yz/xz} < Z_{xy}$ ). In this work we explore the origin of orbital dependent quasiparticle renormalization induced by a suppression of oxygen octahedral rotation that is relevant to the physics of strong correlations in Mn doped  $\text{Sr}_3\text{Ru}_2\text{O}_7$ .

Following the suppression of oxygen octahedral rotation with Mn doping and formation of a correlation induced metal-insulator transition, the temperature-doping phase diagram of  $\text{Sr}_3\text{Ru}_2\text{O}_7$  shows the emergence of a stripe AFM state at the ordering wave vector of  $\mathbf{q}_{AFM} = (\pi/2, \pi/2)$  in a tetragonal unit cell [25]. Recent STM experiments measuring quasiparticle interference (QPI) on the surface of Mn doped  $\text{Sr}_3\text{Ru}_2\text{O}_7$  find that in addition to the structural peaks, a set of four fold symmetric peaks form at the magnetic ordering wave vectors  $\mathbf{q} = (\pm\pi/2, \pm\pi/2)$ . These peaks are found to be highly dispersive both as a function of energy and Mn doping [31]. Interestingly, the origin of these AFM peaks is unexpected in QPI experiments since the measurement is insensitive to a magnetic contrast. Additionally, the observed fourfold

symmetric structure of the QPI peaks would not agree with the stripe type AFM order since a charge coupling to the local magnetic order parameter can be expected to break the lattice symmetry. In addition to the dispersive magnetic peak whose origin is not understood, the experiment also identified a sharp peak at the  $\mathbf{q}^* = (\pi, 0)$  and equivalent wave vectors that are only weakly dispersive. This peak has been proposed to be a possible signature of a charge ordered state [31].

In the following we utilize a tight binding Hamiltonian for  $\text{Sr}_3\text{Ru}_2\text{O}_7$  that incorporates the effect of Mn doping as a suppression in the hopping matrix element that characterizes the presence of an oxygen octahedral rotation [28,29]. Calculation of dynamic paramagnetic susceptibility with this model showed good agreement with spin fluctuations observed in neutron scattering experiments for both undoped and Mn doped  $\text{Sr}_3\text{Ru}_2\text{O}_7$  compound [29]. To explore the role of electron correlations we use a self-consistent  $U(1)$  slave-spin calculation. We show that the quasiparticle weight in Mn doped  $\text{Sr}_3\text{Ru}_2\text{O}_7$  indeed undergoes a stronger suppression for  $d^{xy}$  orbital with increasing electron correlations. Simultaneously, the incoherence of the  $d^{xy}$  dominated bands leads to an increasing quasi-1D nature of the spectral function. We also compute the quasiparticle interference spectra in the lightly doped compound and find good agreement with scanning tunneling microscopy (STM) experiments.

## II. MODEL

The Mn doped  $\text{Sr}_3\text{Ru}_2\text{O}_7$  can be modeled by a 12 orbital tight binding Hamiltonian that includes the  $t_{2g}$  orbitals,  $(d_{a,l}^{yz}, d_{a,l}^{xz}, d_{a,l}^{xy})$  where  $a$  and  $l$  represent the sub-lattice index and layer index, respectively. The effect of Mn doping is incorporated as an effective suppression of the hopping matrix element  $t_{\text{rot}}$  that acts as a parameter in our calculations. The model has been extracted from a combination of symmetry based approaches and fitting to the ARPES experiments [22,32] for the undoped compound [28]. The tight binding Hamiltonian has been utilized to study physical properties of  $\text{Sr}_3\text{Ru}_2\text{O}_7$  like nematicity near the metamagnetic transition [33], and modeling of neutron scattering experiments [29]. The oxygen octahedral rotation causes a doubling of the unit cell where the two sublattices are connected by the wave vector  $\mathbf{Q} = (\pi, \pi)$ . The bilayer interaction further doubles the unit cell and yields a 12 orbital low energy Hamiltonian. As discussed in Ref. [28], the 12 orbital tight binding Hamiltonian can be reduced to a block diagonal form with bonding and antibonding parts by a combination of gauge transformation ( $d_{a,l}^{yz/xz} \rightarrow -d_{a,l}^{yz/xz}$ ) and Fourier transform on the layer index by introducing the momentum index  $k_z = (0, \pi)$ . This allows us to express the Hamiltonian as

$$H_0 = h_0(k_z = 0) + h_0(k_z = \pi). \quad (1)$$

The detailed Hamiltonian is presented in Appendix A. The formalism thus allows us to work with a reduced  $6 \times 6$  tight-binding Hamiltonian block separately for each  $k_z$  index.

The oxygen octahedral rotation induced by the Mn dopants is controlled by a dominant intersublattice term of the form  $2t_{\text{rot}}(\cos(k_x) + \cos(k_y))d_{\mathbf{k}+\mathbf{Q},a,k_z}^{yz\dagger}d_{\mathbf{k},a',k_z}^{xz}$  as also evidenced in Hamiltonians generated from DFT calculations [34]. Increasing Mn doping is modeled as a corresponding suppression

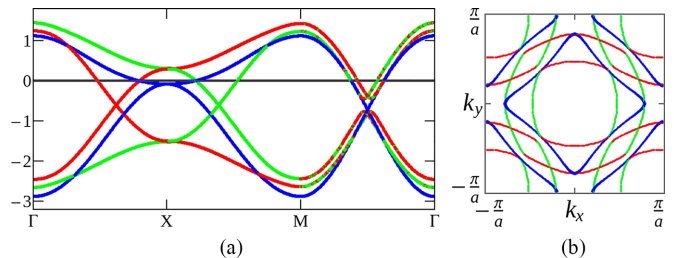


FIG. 1. Band structure (a) and Fermi-surface (b) for  $t_{\text{rot}} = 0.4$ . Red, green, and blue colors correspond to  $d^{yz}$ ,  $d^{xz}$ , and  $d^{xy}$  bands, respectively.

in  $t_{\text{rot}}$ . The electronic structure based on this tight-binding Hamiltonian and the Fermi-surface for the undoped compound ( $t_{\text{rot}} = 0.4$ ) are shown in Fig. 1. As can be seen from Fig. 1(a), apart from the  $d^{yz/xz}$  orbital dominated bands shown in red/blue, the electronic structure of the undoped material has a  $d^{xy}$  orbital contribution (blue) that leads to a high density of states near the X point of the Brillouin zone. The energy scale is expressed in units of 0.6 eV.

To study the effect of electron correlations, we utilize a self-consistent  $U(1)$  slave-spin formalism [35]. The slave particle methods can account for many details of the quasiparticle physics close to the Fermi energy for strongly interacting multi-orbital systems with modest effort compared to more numerically expensive methods, like quantum Monte Carlo, within the dynamical mean field theory framework. The slave-spin formalism can obtain the Mott phase in agreement with DMFT methods [36] and the  $U(1)$  formalism at the mean field levels can capture the noninteracting limit accurately [37]. Below we summarize the calculation method using the  $U(1)$  slave-spin formalism employed in our work.

For the charge degrees of freedom represented by a quantum spin  $1/2$ , the electron operator can be written as

$$d_{i\alpha\sigma}^\dagger = S_{i\alpha\sigma}^+ f_{i\alpha\sigma}^\dagger, \quad (2)$$

where  $i$ ,  $\alpha$ , and  $\sigma$  stand for the site index, orbital index, and the spin index, respectively. The creation of charge on the site  $i$ , with orbital  $\alpha$  and spin  $\sigma$ , is described by the spin raising operator for the slave-spin  $S_{i\alpha\sigma}^+ \cdot f_{i\alpha\sigma}^\dagger$  represents the fermionic spinon corresponding to the physical spin. The mean field equations are then solved subject to removing the unphysical states from the Hilbert space using the constraint equation:

$$S_{i\alpha\sigma}^z = f_{i\alpha\sigma}^\dagger f_{i\alpha\sigma} - \frac{1}{2} \quad (3)$$

where  $S_{i\alpha\sigma}^z$  is the  $z$  component of the spin operator (see Appendix B for further details). The orbital dependant quasiparticle weights are obtained as

$$z_{\alpha\sigma} = \langle S_{i\alpha\sigma}^+ \rangle. \quad (4)$$

The correlated metallic phase is given by  $z_{\alpha\sigma} \neq 0$  whereas the orbital-selective Mott transition (OSMT) phase is described by  $z_{\alpha\sigma} = 0$  for some orbitals. The calculations have been performed at  $T = 0$  and describe the nonmagnetic states where  $Z_{\alpha\sigma} = Z_\alpha$ . From the above one may note that the OSMT is not a complete Mott insulating phase but describes a correlated metal where certain orbital resolved QP weights are still finite. This makes the model ideal for studying the OSMT state in

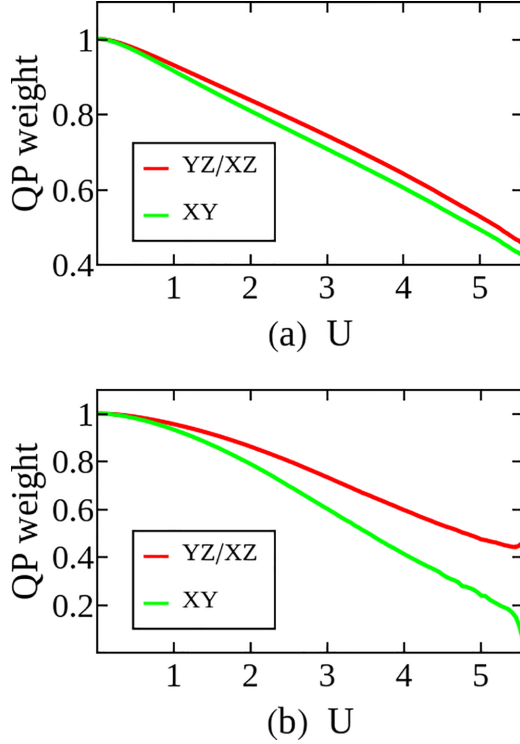


FIG. 2. Orbital resolved quasiparticle weight vs coulomb energy  $U$  for  $t_{\text{rot}} = 0.1$  at (a)  $J = 0$  and (b)  $J = 0.2U$ .

$\text{Sr}_3\text{Ru}_2\text{O}_7$  near  $x \sim 0.05$  doping since the material is still in the paramagnetic phase.

### III. RESULTS

In order to model the reduced octahedral rotation with Mn doping we take  $t_{\text{rot}} = 0.1$  [29]. Although  $t_{\text{rot}}$  is a parameter in our study,  $t_{\text{rot}} = 0.1$  corresponds to the regime where the Fermi surface shows quasi-1D behavior observed in ARPES experiments [3], and a paramagnetic susceptibility that peaks at the correct wave vector for the AFM order observed in doped  $\text{Sr}_3\text{Ru}_2\text{O}_7$  [29]. We also find that at these small values of  $t_{\text{rot}}$ , our results remain robust with small changes of  $t_{\text{rot}}$  magnitude.

The self-consistent solution obtained from the  $U(1)$  slave-spin formalism with increasing Hubbard-interaction  $U$  for exchange coupling strengths  $J = 0$ , and  $J = 0.2U$  are shown in Figs. 2(a) and 2(b), respectively. We observe a transition to an orbital selective phase where the  $d^{xy}$  orbital weight  $Z_{xy}$  is suppressed compared to the  $d^{yz/xz}$  orbital quasiparticle weights  $Z_{yz/xz}$ . This scenario is contrary to the case of undoped  $\text{Sr}_3\text{Ru}_2\text{O}_7$  where the orbital selectivity is much weaker, and  $Z_{yz/xz} < Z_{xy}$  [30]. These results are in agreement with recent ARPES experiments that find an emergence of orbital selective Mott transition in Mn doped  $\text{Sr}_3\text{Ru}_2\text{O}_7$ , where the  $d^{xy}$  orbital dominated band is observed to become incoherent at low temperatures [3]. As shown in Fig. 2, with the increases in  $J$  the critical  $U$  for the Mott transition is reduced due to increasing electron correlations. We also find that the orbital selective splitting between the  $d^{yz/xz}$  and  $d^{xy}$  orbitals is enhanced in the presence of larger exchange interaction  $J$ .

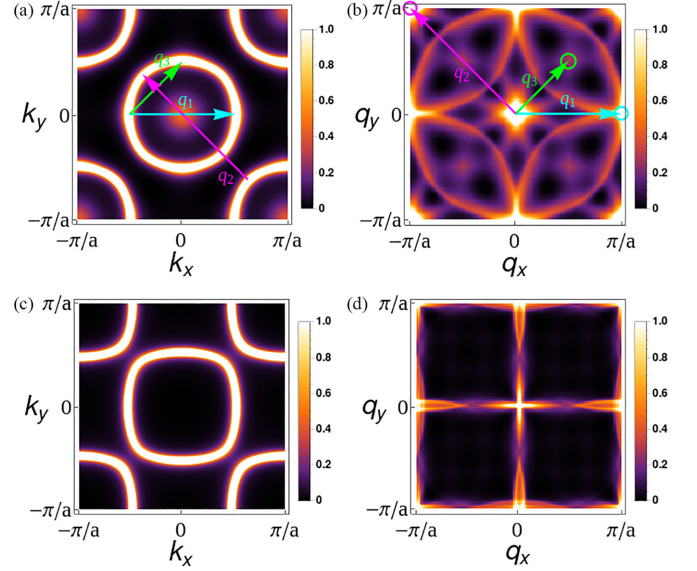


FIG. 3. Calculation of spectral function and QPI at  $\omega = 0$  for  $t_{\text{rot}} = 0.1$ . Top row: spectral function (a) and QPI (b) at  $Z_{yz/xz} = 0.4$ ,  $Z_{xy} = 0.1$ . Bottom row: spectral function (c) and QPI (d) at  $Z_{yz/xz} = 0.4$ ,  $Z_{xy} = 0$ . Here,  $a$  is the lattice constant in tetragonal unit cell. The variables  $\mathbf{k}$  and  $\mathbf{q}$  are presented in r.l.u.

In order to understand the evolution of the Fermi-surface with increasing incoherence of the  $d^{xy}$  orbital, we evaluate the spectral function by calculating the retarded Green's function in the Lehman representation [37,38],

$$G_{\alpha,\sigma,\lambda}^{\text{ret}}(\mathbf{k}, \omega) = \frac{1}{N} \sum_{n,m} |\langle n | S_{\alpha\sigma}^+ | m \rangle|^2 (U_{k\sigma}^{\alpha\lambda})^* U_{k\sigma}^{\alpha\lambda} \times \frac{[e^{-\beta E_m} (1 - n_{\lambda}^f(\mathbf{k})) + e^{-\beta E_n} n_{\lambda}^f(\mathbf{k})]}{\omega + i\eta - (E_n - E_m) - \epsilon_{\lambda}(\mathbf{k})}. \quad (5)$$

Here,  $\epsilon_{\lambda}(\mathbf{k})$  and  $E_m$  are the eigenvalues, whereas  $U_{k\sigma}^{\alpha\lambda}$  and  $|m\rangle$  are the eigenstates of the spinon mean field Hamiltonian  $H^f$  and slave-spin Hamiltonian  $H^s$ , respectively. The term  $n_{\lambda}^f(\mathbf{k})$  is the Fermi distribution function that corresponds to band  $\lambda$  with momentum  $\mathbf{k}$ . The spectral function is then given by the coherent part of the retarded Green's function (corresponding to  $n = m$ ):

$$A_{\alpha\sigma}(\mathbf{k}, \omega) = -2 \sum_{\lambda} \text{Im} G_{\alpha,\sigma,\lambda}^{\text{ret}}(\mathbf{k}, \omega). \quad (6)$$

The computed spectral function at  $\omega = 0$  and  $Z_{yz/xz} = 0.4$ ,  $Z_{xy} = 0.1$  shown in Fig. 3(a) is compared to the orbital selective Mott phase corresponding to  $Z_{yz/xz} = 0.4$ ,  $Z_{xy} = 0$  in Fig. 3(c). In agreement with ARPES experiments we find that the spectral function of the interacting system becomes more quasi-1D as the octahedral rotation is suppressed and the  $d^{xy}$  orbital becomes incoherent. This is expected to occur because of the quasi-1D nature of the  $d^{yz/xz}$  orbitals. However, note that there is presence of a hybridization between the  $d^{xz}$  and  $d^{yz}$  orbitals through a next nearest neighbor intrasublattice hopping matrix element and via the spin orbit coupling (see Appendix A). This hybridization, combined with weak but finite intraorbital nearest neighbor hybridization within the

$d^{yz/xz}$  orbitals along the  $(x/y)$  directions, respectively, provide for a small but finite warping of the quasi-1D bands even in the absence of the  $d^{xy}$  band.

To gain further insight into the role of electron correlations in this Mn doped  $\text{Sr}_3\text{Ru}_2\text{O}_7$  we model the QPI experiments. Recent QPI experiments [31] in the region of OSMT find three distinctive peaks at the  $(\pi, \pi)$ ,  $(\pi, 0)$ , and  $(\pi/2, \pi/2)$  wave vectors. Whereas the  $(\pi, \pi)$  peak could be associated with the structural symmetry, the  $(\pi, 0)$  peak has been ascribed to the presence of a possible charge ordered state, and the observed  $(\pm\pi/2, \pm\pi/2)$  QPI peak coincides with the magnetic wave vector of the stripe magnetic order in the presence of Mn doping [25,31]. The QPI spectrum can be extracted from the calculation of joint density of states (JDOS),

$$\text{JDOS}(\mathbf{q}, \omega) = \frac{1}{N} \sum_{\mathbf{k}\alpha\sigma} A_{\alpha\sigma}(\mathbf{k} + \mathbf{q}, \omega) A_{\alpha\sigma}(\mathbf{k}, \omega) \quad (7)$$

where,  $N$  is a normalization factor. From Eq. (5) and Eq. (6), we find that the single particle Green's function and correspondingly the QPI spectra is expected to be influenced by the presence of orbital dependant renormalization of the Landau quasiparticles. In Fig. 3, we show the QPI spectra at the Fermi energy ( $\omega = 0$ ) relevant to Mn doped  $\text{Sr}_3\text{Ru}_2\text{O}_7$ . For  $Z_{xy} = 0.1$  in Fig. 3(b), QPI peaks can be seen at the three wave vectors  $\mathbf{q}_1 = (\pi, 0)$ ,  $\mathbf{q}_2 = (\pi, \pi)$ , and  $\mathbf{q}_3 = (\pi/2, \pi/2)$  that agree well with corresponding observations in  $x \sim 5\%$  Mn doped  $\text{Sr}_3\text{Ru}_2\text{O}_7$  [31]. As shown in Fig. 3(a), the curvature of the  $\Gamma$ -centered pocket near the  $(\pm\pi/2, 0)$  and  $(0, \pm\pi/2)$  region are responsible for the enhanced joint density of state at the  $\mathbf{q}_1$  and  $\mathbf{q}_3$  wave vectors. The presence of a QPI peak at the AFM wave vector in the paramagnetic phase explains the presence of a fourfold symmetry in this peak as observed in the experiments.

As the system is further Mn doped, an OSMT phase is obtained where  $Z_{xy} \rightarrow 0$ . As shown in Fig. 3(d) for the case of  $Z_{yz/xz} = 0.4$ , and  $Z_{xy} = 0$ , this causes the  $\mathbf{q}_3 = (\pi/2, \pi/2)$  to strongly disperse. The vanishing of this  $\mathbf{q}_3$  peak can also be understood from the constant energy contour in Fig. 3(c), the quasi-1D nature of the Fermi pockets suppresses the curvature of the inner pocket near the  $(\pm\pi/2, 0)$  and  $(0, \pm\pi/2)$  points, leading to suppression of the JDOS at the antiferromagnetic wave vector. However, we find that the  $\mathbf{q}_1$  and the  $\mathbf{q}_2$  peaks survive and are in fact strengthened with the formation of the quasi-1D bands. These QPI peaks and their dispersion are in agreement with the experiments on doped  $\text{Sr}_3\text{Ru}_2\text{O}_7$  [31].

In Fig. 4(a) and Fig. 4(b) we compare the spectral function and QPI spectra obtained above with those obtained from the noninteracting Hamiltonian in doped  $\text{Sr}_3\text{Ru}_2\text{O}_7$  ( $t_{\text{rot}} = 0.1$ , and  $U = 0$ ) at  $\omega = 0$ . This spectra will be qualitatively similar to the effect observed at the Fermi energy when the quasiparticle renormalizations are not orbitally selective ( $U > 0$ , and  $Z_{yz/xz} = Z_{xy}$ ). Note that in this case we do not obtain the quasi-1D nature of spectral function [see Fig. 4(a)]. Similarly, for the QPI spectra in Fig. 4(b) we also do not obtain the observed peaks at the  $\mathbf{q}_1$ ,  $\mathbf{q}_2$ ,  $\mathbf{q}_3$  wave vectors. This indicates the relevance of accounting for the orbitally selective Mott physics to understand the low energy electronic structure in Mn doped  $\text{Sr}_3\text{Ru}_2\text{O}_7$ . However, it can be seen from Fig. 4(b) that the 1D enhancement of the JDOS along the  $(q_x, 0)$ , and

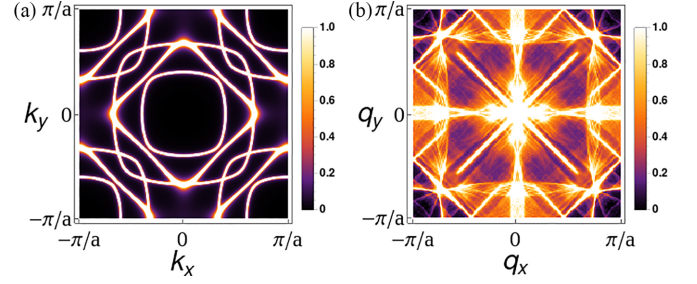


FIG. 4. Calculation of (a) spectral function and (b) QPI spectra at  $\omega = 0$ ,  $t_{\text{rot}} = 0.1$ , and  $Z_{yz/xz} = 1$ ,  $Z_{xy} = 1$ .

$(0, q_y)$  is present in the QPI spectra in the OSMT phase shown in Fig. 3(d). This implies the dominant mechanism for the formation of these quasi-1D regions are the reduced inter-orbital hybridization  $t_{\text{rot}}$  between  $d_{xz}$  and  $d_{yz}$  orbitals. Similar quasi-1D enhancements in QPI intensity have been observed in measurements in the  $x \sim 10\%$  samples studied in Ref. [31].

We further looked at the energy dependence of QPI spectrum at  $\omega = \pm 0.02$  as shown in Fig. 5. At finite energies the QPI peak at  $\mathbf{q}_1$  and  $\mathbf{q}_2$  wave vectors are observed but the peak at the AFM wave vector is suppressed. We also find that for the QPI spectra in the OSMT phase, the QPI intensity shows quasi-1D features for small positive energies but similar to experiments it is suppressed for  $\omega < 0$ . A generic intensity enhancement along the lines  $\mathbf{q} = (0, q_y)/(q_x, 0)$  will in general be dominated by contributions from the  $d_{yz/xz}$  orbitals (even for  $Z_{xy} > 0$ ) and represents the quasi-1D nature of the spectral function in Mn doped  $\text{Sr}_3\text{Ru}_2\text{O}_7$ .

#### IV. CONCLUSION

We have studied the effect of strong electron correlations in Mn doped  $\text{Sr}_3\text{Ru}_2\text{O}_7$ . The effect of Mn doping is simulated through a suppression of oxygen octahedral rotation that is modeled with a suppression of the parameter  $t_{\text{rot}}$ . We utilize a self-consistent  $U(1)$  slave-spin formulation that allows us to probe the low energy properties of the doped material. The orbital resolved quasiparticle weight shows the emergence of an OSMT phase where  $Z_{xy} < Z_{yz/xz}$ . As a consequence of the suppression of the  $d_{xy}$  orbital quasiparticle weight, the spectral function develops quasi-1D features similar to observations in ARPES experiments.

We further evaluate the QPI spectra within this orbital selective phase and find clear evidence of enhanced JDOS at the wave vectors  $\mathbf{q}_1 = (\pi, 0)$ ,  $\mathbf{q}_2 = (\pi, \pi)$ , and  $\mathbf{q}_3 = (\pi/2, \pi/2)$  similar to observations from STM experiments. In particular, we find that the presence of the  $\mathbf{q}_1 = (\pi, 0)$  and  $\mathbf{q}_3 = (\pi/2, \pi/2)$  intensities in QPI calculations does not require the explicit presence of a charge ordered and AFM state. However, whereas the QPI peaks correspond to high curvature regions of the constant energy contours [Figs. 3(a) and 3(b)], the Fermi pockets also form flat regions that could enhance nesting at the above wave vectors and support the formation of density wave instabilities.

The  $\mathbf{q}_3$  peak is suppressed as  $t_{\text{rot}} \rightarrow 0$  and  $Z_{xy} \rightarrow 0$ , in agreement with QPI experiments [31]. Further, this peak is strongly suppressed for small but finite energies, although the  $\mathbf{q}_1$  and  $\mathbf{q}_2$  peaks remain robust.

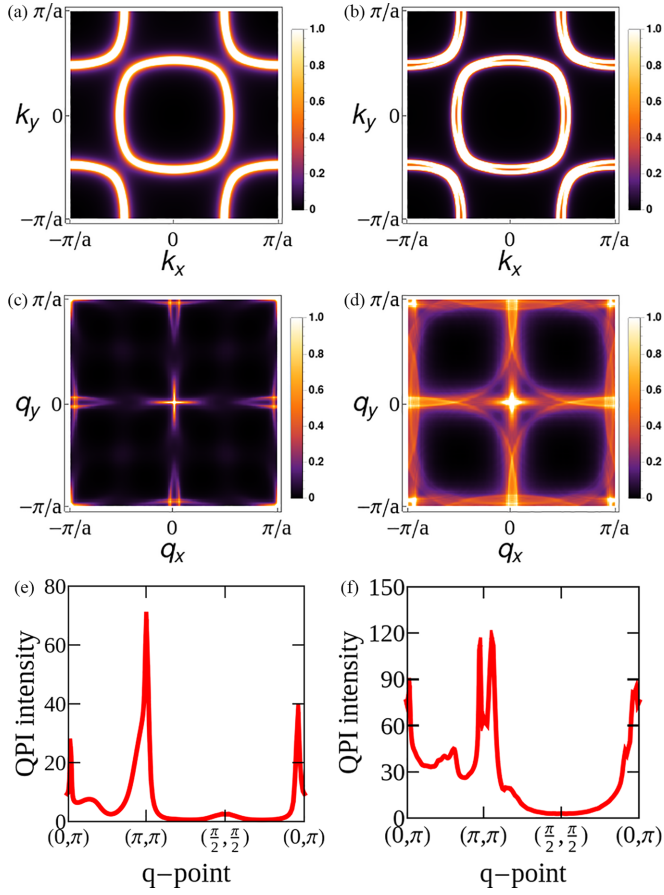


FIG. 5. Calculation of spectral function and QPI at  $Z_{yz/xz} = 0.4$ , and  $Z_{xy} = 0$  for energies  $\omega = -0.02$  (Left column) and  $\omega = 0.02$  (Right column) ( $\omega$  is in 600 meV unit): (a) and (b) are the spectral functions at the two energies. The panels (c) and (d) show the QPI spectra at the above energies for which the corresponding plots along high symmetry paths are shown in (e) and (f). The plots have been constructed in a tetragonal unit cell with lattice constant  $a$ . The momentum space vectors  $\mathbf{k}$  and  $\mathbf{q}$  are presented in r.l.u.

In summary, we find that the modeling of Mn doped  $\text{Sr}_3\text{Ru}_2\text{O}_7$  used in our study can reproduce the experimentally observed spectral function and QPI peaks as well as the quasi-1D enhancement of JDOS along the  $(q_x, 0)$  and  $(0, q_y)$  regions. The orbital resolved quasiparticle weight splitting between the  $Z_{xz/yz}$  and  $Z_{xy}$ , and the critical  $U$  for orbital selective Mott transition increase with Hund's coupling  $J$ . The choice of  $J = 0.2U$  is based on the experimentally observed renormalization of the  $d_{xz/yz}$  orbital dominated bands in the orbitally selective Mott phase [3].

The spectral function and quasiparticle interference spectra are strongly influenced by electron correlation effects that lead to an orbitally selective Mott phase in addition to the role of reduced oxygen octahedral rotation in modifying the electronic structure in Mn doped  $\text{Sr}_3\text{Ru}_2\text{O}_7$ . These results will have significance in other strongly correlated materials where oxygen octahedral rotation and strong correlation physics are being studied, including surface of unconventional superconductor  $\text{Sr}_2\text{RuO}_4$  [39], infinite layer nickelates [40], and recent work in Ca doped  $\text{Sr}_2\text{RuO}_4$  where experiments find an intricate relationship between OSMT physics and oxygen octahedral distortions [41].

## ACKNOWLEDGMENT

S.M. acknowledges financial support by Science and Engineering Research Board (SERB), Department of Science and Technology, Ministry of Science and Technology, India through the MATRICS Grant No. MTR/2020/000524.

## APPENDIX A: TIGHT BINDING HAMILTONIAN

As discussed above, the tight binding Hamiltonian [28] for Mn doped  $\text{Sr}_3\text{Ru}_2\text{O}_7$  can be written in block diagonal form for  $k_z = 0$  and  $k_z = \pi$ . The Hamiltonian can be expressed as

$$h_0(k_z) = \sum_{\mathbf{k}} \phi_{\mathbf{k},s,k_z}^\dagger \begin{pmatrix} \hat{h}_{0s}(\mathbf{k}, k_z) & \hat{g}^\dagger(\mathbf{k}, k_z) \\ \hat{g}(\mathbf{k}, k_z) & \hat{h}_{0s}(\mathbf{k} + \mathbf{Q}, k_z) \end{pmatrix} \phi_{\mathbf{k},s,k_z}, \quad (\text{A1})$$

where the basis is given by

$$\phi_{\mathbf{k},s,k_z}^\dagger = (d_{\mathbf{k},s,k_z}^{yz\dagger}, d_{\mathbf{k},s,k_z}^{xz\dagger}, d_{\mathbf{k},-s,k_z}^{xy\dagger}, d_{\mathbf{k}+\mathbf{Q},s,k_z}^{yz\dagger}, d_{\mathbf{k}+\mathbf{Q},s,k_z}^{xz\dagger}, d_{\mathbf{k}+\mathbf{Q},-s,k_z}^{xy\dagger}), \quad (\text{A2})$$

where  $d_{\mathbf{k},s,k_z}^{\alpha\dagger}$  creates an electron in orbital  $\alpha$  of Ru ion with spin  $s$ . Here,  $\mathbf{k} = (k_x, k_y)$  is the in-plane momentum index. The sublattices are described by the ordering vector  $\mathbf{Q} = (\pi, \pi)$ .

The individual Hamiltonian components,  $\hat{h}_{0s}(\mathbf{k}, k_z)$  and  $\hat{g}(\mathbf{k}, k_z)$ , are given by

$$\hat{h}_{0s}(\mathbf{k}, k_z) = \hat{A}_s(\mathbf{k}) + \hat{B}_1 \cos(k_z), \quad (\text{A3})$$

$$\hat{g}(\mathbf{k}, k_z) = \hat{G}(\mathbf{k}) - 2\hat{B}_2 \cos(k_z). \quad (\text{A4})$$

Here, the matrix kernel  $\hat{A}_s(\mathbf{k})$  is intralayer hopping without oxygen octahedral rotation, and  $\hat{G}(\mathbf{k})$  contains the contribution from in-plane staggered hopping. The interlayer hoppings with and without octahedral rotation are given by  $\hat{B}_2$  and  $\hat{B}_1$ , respectively [28]. The individual matrix elements are given by

$$\hat{A}_s(\mathbf{k}) = \begin{pmatrix} \epsilon_{\mathbf{k}}^{yz} & \epsilon_{\mathbf{k}}^{\text{off}} + is\lambda & 0 \\ \epsilon_{\mathbf{k}}^{\text{off}} - is\lambda & \epsilon_{\mathbf{k}}^{xz} & 0 \\ 0 & 0 & \epsilon_{\mathbf{k}}^{xy} \end{pmatrix}, \quad (\text{A5})$$

$$\hat{G}(\mathbf{k}) = \begin{pmatrix} 0 & 2t_{\text{rot}}\gamma k & 0 \\ -2t_{\text{rot}}\gamma k & 0 & 0 \\ 0 & 0 & 0 \end{pmatrix}, \quad (\text{A6})$$

$$\hat{B}_1 = \begin{pmatrix} -t_{\perp} & 0 & 0 \\ 0 & -t_{\perp} & 0 \\ 0 & 0 & 0 \end{pmatrix}, \quad (\text{A7})$$

$$\hat{B}_2 = \begin{pmatrix} 0 & t_{\text{INT}}^{\perp} & 0 \\ -t_{\text{INT}}^{\perp} & 0 & 0 \\ 0 & 0 & 0 \end{pmatrix}. \quad (\text{A8})$$

In the above expressions the components are given by

$$\epsilon_{\mathbf{k}}^{yz} = -2t_2 \cos(k_x) - 2t_1 \cos(k_y), \quad (\text{A9})$$

$$\epsilon_{\mathbf{k}}^{xz} = -2t_1 \cos(k_x) - 2t_2 \cos(k_y), \quad (\text{A10})$$

$$\begin{aligned} \epsilon_k^{xy} = & -2t_3[\cos(k_x) + \cos(k_y)] \\ & -4t_4 \cos(k_x) \cos(k_y) \\ & -2t_5[\cos(2k_x) + \cos(2k_y)], \end{aligned} \quad (\text{A11})$$

$$\epsilon_k^{\text{off}} = -4t_6 \sin(k_x) \sin(k_y), \quad (\text{A12})$$

$$\gamma_k = \cos(k_x) + \cos(k_y). \quad (\text{A13})$$

The tight binding Hamiltonian is expressed in the tetragonal unit cell and all the hopping parameters are in the unit of 600 meV. The value of hopping parameters are given by  $t_1 = 0.5$ ,  $t_2 = 0.05$ ,  $t_3 = 0.3$ ,  $t_4 = 0.06$ ,  $t_5 = -0.018$ ,  $t_6 = 0.05$ ,  $\lambda = 0.1$ ,  $t_{\perp} = 0.005$ , and  $t_{\text{INT}}^{\perp} = 0.005$ .

### APPENDIX B: $U(1)$ SLAVE-SPIN MODEL

We include an on site, multi-orbital Hubbard-Hund Hamiltonian where the correlation term is given by [1,38,42]

$$\begin{aligned} H_U = & U \sum_{i\alpha} \hat{n}_{i\alpha\uparrow} \hat{n}_{i\alpha\downarrow} + \frac{U'}{2} \sum_{i,\alpha\neq\beta} \sum_{\sigma} \hat{n}_{i\alpha\sigma} \hat{n}_{i\beta\sigma} \\ & + \frac{U' - J}{2} \sum_{i,\alpha\neq\beta} \sum_{\sigma} \hat{n}_{i\alpha\sigma} \hat{n}_{i\beta\sigma} + H_{\text{pair}} + H_{\mu_d}, \end{aligned} \quad (\text{B1})$$

where  $c_{i\alpha\sigma}^{\dagger}$  corresponds to the electron creation at site  $i$  of Ruthenium  $t_{2g}$  orbitals  $\alpha$ ,  $\beta$ , and spin  $\sigma = \uparrow, \downarrow$ . The first term  $U$  accounts for the intraorbital Coulomb interaction, the Hund's interaction is given by  $J$ , and the interorbital Coulomb interaction for opposite spin is given by  $U' = U - 2J$ . The term  $\hat{n}_{i\alpha\sigma} = c_{i\alpha\sigma}^{\dagger} c_{i\alpha\sigma}$  is the electron occupation for orbital  $\alpha$  and spin  $\sigma$ . The additional term  $H_{\text{pair}}$  is a pair hopping term [38] given by

$$\begin{aligned} H_{\text{pair}} = & -\frac{J}{2} \sum_{i,\alpha\neq\beta} [c_{i\alpha\uparrow}^{\dagger} c_{i\alpha\downarrow} c_{i\beta\downarrow}^{\dagger} c_{i\beta\uparrow} \\ & + c_{i\alpha\uparrow}^{\dagger} c_{i\alpha\downarrow}^{\dagger} c_{i\beta\uparrow} c_{i\beta\downarrow} + \text{H.c.}] \end{aligned} \quad (\text{B2})$$

and,

$$H_{\mu_d} = -\mu_d^U \sum_{i\alpha\sigma} \hat{n}_{i\alpha\sigma}. \quad (\text{B3})$$

Within a  $U(1)$  slave-spin formalism we associate the Hilbert space containing the charge degree of freedom with an auxiliary fermion containing the degree of freedom of the physical spin [35,38,43]. Under these conditions, the electron creation operator will take the form

$$c_{i\alpha\sigma}^{\dagger} = S_{i\alpha\sigma}^{+} f_{i\alpha\sigma}^{\dagger}, \quad (\text{B4})$$

where  $i$ ,  $\alpha$ , and  $\sigma$  stand for the site index, orbital index, and the spin index, respectively. According to the formulation of the Hilbert space, the charge degree of freedom follows the spin half algebra where the  $S_{i\alpha\sigma}^{+}$  behaves as the charge creation operator which takes the empty state (zero charge) to a filled state ( $-e$  charge). So, here the physical states should look like [44]:

$$|0\rangle = |n_{i\alpha\sigma}^f = 0, S_{i\alpha\sigma}^z = -1/2\rangle, \quad (\text{B5})$$

$$|1\rangle = |n_{i\alpha\sigma}^f = 1, S_{i\alpha\sigma}^z = 1/2\rangle. \quad (\text{B6})$$

There should obviously be some extra nonphysical states like  $|n_{i\alpha\sigma}^f = 1, S_{i\alpha\sigma}^z = -1/2\rangle$ , which could be eliminated by introducing the constraint

$$S_{i\alpha\sigma}^z = f_{i\alpha\sigma}^{\dagger} f_{i\alpha\sigma} - \frac{1}{2}. \quad (\text{B7})$$

The constraint equation is averaged over all sites and introduced in the Hamiltonian by introducing Lagrange multipliers. Upon a mean field decomposition, the Hamiltonian is reduced into a spinon Hamiltonian ( $H^f$ ) and a slave-spin Hamiltonian ( $H^s$ ), which are solved self-consistently to calculate the mean field parameter like  $z_{\alpha\sigma}$ . The quasiparticle weight is calculated to be

$$Z_{\alpha\sigma} = |z_{\alpha\sigma}|^2. \quad (\text{B8})$$

- 
- [1] R. Yu and Q. Si, *Phys. Rev. Lett.* **110**, 146402 (2013).  
[2] M. Neupane, P. Richard, Z.-H. Pan, Y.-M. Xu, R. Jin, D. Mandrus, X. Dai, Z. Fang, Z. Wang, and H. Ding, *Phys. Rev. Lett.* **103**, 097001 (2009).  
[3] M. Nakayama, T. Kondo, K. Kuroda, C. Bareille, M. D. Watson, S. Kunisada, R. Noguchi, T. K. Kim, M. Hoesch, Y. Yoshida, and S. Shin, *Phys. Rev. B* **98**, 161102(R) (2018).  
[4] T. Kondo, M. Ochi, M. Nakayama, H. Taniguchi, S. Akebi, K. Kuroda, M. Arita, S. Sakai, H. Namatame, M. Taniguchi *et al.*, *Phys. Rev. Lett.* **117**, 247001 (2016).  
[5] M. Yi, Z.-K. Liu, Y. Zhang, R. Yu, J.-X. Zhu, J. J. Lee, R. G. Moore, F. T. Schmitt, W. Li, S. C. Riggs *et al.*, *Nat. Commun.* **6**, 7777 (2015).  
[6] D. Sutter, M. Kim, C. E. Matt, M. Horio, R. Fittipaldi, A. Vecchione, V. Granata, K. Hauser, Y. Sassa, G. Gatti, M. Griioni, M. Hoesch, T. K. Kim, E. Rienks, N. C. Plumb, M. Shi, T. Neupert, A. Georges, and J. Chang, *Phys. Rev. B* **99**, 121115(R) (2019).  
[7] L. de'Medici, *Phys. Rev. B* **83**, 205112 (2011).  
[8] A. Georges, L. d. Medici, and J. Mravlje, *Annu. Rev. Condens. Matter Phys.* **4**, 137 (2013).  
[9] L. de'Medici, S. R. Hassan, M. Capone, and X. Dai, *Phys. Rev. Lett.* **102**, 126401 (2009).  
[10] J. Herbrych, N. Kaushal, A. Nocera, G. Alvarez, A. Moreo, and E. Dagotto, *Nat. Commun.* **9**, 3736 (2018).  
[11] N. Patel, A. Nocera, G. Alvarez, A. Moreo, S. Johnston, and E. Dagotto, *Commun. Phys.* **2**, 64 (2019).  
[12] J. Rincón, A. Moreo, G. Alvarez, and E. Dagotto, *Phys. Rev. Lett.* **112**, 106405 (2014).  
[13] S. Koley, M. S. Laad, N. S. Vidhyadhiraja, and A. Taraphder, *Phys. Rev. B* **90**, 115146 (2014).  
[14] A. Kreisel, B. M. Andersen, and P. J. Hirschfeld, *Phys. Rev. B* **98**, 214518 (2018).  
[15] P. O. Sprau, A. Kostin, A. Kreisel, A. E. Böhmer, V. Taufour, P. C. Canfield, S. Mukherjee, P. J. Hirschfeld, B. M. Andersen, and J. S. Davis, *Science* **357**, 75 (2017).

- [16] R. Yu, H. Hu, E. M. Nica, J.-X. Zhu, and Q. Si, *Front. Phys.* **9**, 578347 (2021).
- [17] D. O. Brodsky, M. E. Barber, J. A. Bruin, R. A. Borzi, S. A. Grigera, R. S. Perry, A. P. Mackenzie, and C. W. Hicks, *Sci. Adv.* **3**, e1501804 (2017).
- [18] C. Lester, S. Ramos, R. Perry, T. Croft, R. Bewley, T. Guidi, P. Manuel, D. Khalyavin, E. Forgan, and S. Hayden, *Nat. Mater.* **14**, 373 (2015).
- [19] C. Lester, S. Ramos, R. Perry, T. Croft, M. Laver, R. Bewley, T. Guidi, A. Hiess, A. Wildes, E. Forgan *et al.*, *Nat. Commun.* **12**, 5798 (2021).
- [20] M. Zhu, Y. Wang, P. G. Li, J. J. Ge, W. Tian, D. Keavney, Z. Q. Mao, and X. Ke, *Phys. Rev. B* **95**, 174430 (2017).
- [21] P. Rivero, R. Jin, C. Chen, V. Meunier, E. Plummer, and W. Shelton, *Sci. Rep.* **7**, 10265 (2017).
- [22] M. P. Allan, A. Tamai, E. Rozbicki, M. Fischer, J. Voss, P. King, W. Meevasana, S. Thirupathiah, E. Rienks, J. Fink *et al.*, *New J. Phys.* **15**, 063029 (2013).
- [23] R. Nepal, L. Xing, A. Meingast, and R. Jin, *Phys. Rev. Res.* **3**, 043183 (2021).
- [24] B. Hu, G. T. McCandless, V. O. Garlea, S. Stadler, Y. Xiong, J. Y. Chan, E. W. Plummer, and R. Jin, *Phys. Rev. B* **84**, 174411 (2011).
- [25] D. Mesa, F. Ye, S. Chi, J. A. Fernandez-Baca, W. Tian, B. Hu, R. Jin, E. W. Plummer, and J. Zhang, *Phys. Rev. B* **85**, 180410(R) (2012).
- [26] R. Mathieu, A. Asamitsu, Y. Kaneko, J. P. He, X. Z. Yu, R. Kumai, Y. Onose, N. Takeshita, T. Arima, H. Takagi, and Y. Tokura, *Phys. Rev. B* **72**, 092404 (2005).
- [27] M. A. Hossain, B. Bohnenbuck, Y. D. Chuang, M. W. Haverkort, I. S. Elfimov, A. Tanaka, A. G. Cruz Gonzalez, Z. Hu, H.-J. Lin, C. T. Chen, R. Mathieu, Y. Tokura, Y. Yoshida, L. H. Tjeng, Z. Hussain, B. Keimer, G. A. Sawatzky, and A. Damascelli, *Phys. Rev. B* **86**, 041102(R) (2012).
- [28] W.-C. Lee, D. P. Arovas, and C. Wu, *Phys. Rev. B* **81**, 184403 (2010).
- [29] S. Mukherjee and W.-C. Lee, *Phys. Rev. B* **94**, 064407 (2016).
- [30] C. Piefke and F. Lechermann, *Phys. Status Solidi B* **248**, 2269 (2011).
- [31] J. Leshen, M. Kavai, I. Giannakis, Y. Kaneko, Y. Tokura, S. Mukherjee, W.-C. Lee, and P. Aynajian, *Commun. Phys.* **2**, 36 (2019).
- [32] A. Tamai, M. P. Allan, J. F. Mercure, W. Meevasana, R. Dunkel, D. H. Lu, R. S. Perry, A. P. Mackenzie, D. J. Singh, Z.-X. Shen, and F. Baumberger, *Phys. Rev. Lett.* **101**, 026407 (2008).
- [33] C. M. Puetter, J. G. Rau, and H.-Y. Kee, *Phys. Rev. B* **81**, 081105(R) (2010).
- [34] C. Autieri, M. Cuoco, and C. Noce, *Phys. Rev. B* **89**, 075102 (2014).
- [35] R. Yu and Q. Si, *Phys. Rev. B* **86**, 085104 (2012).
- [36] L. de'Medici, A. Georges, and S. Biermann, *Phys. Rev. B* **72**, 205124 (2005).
- [37] R. Yu and Q. Si, *Phys. Rev. B* **84**, 235115 (2011).
- [38] W.-C. Lee, M. J. Wahila, S. Mukherjee, C. N. Singh, T. Eustance, A. Regoutz, H. Paik, J. E. Boschker, F. Rodolakis, T.-L. Lee *et al.*, *J. Appl. Phys.* **125**, 082539 (2019).
- [39] A. Kreisel, C. Marques, L. Rhodes, X. Kong, T. Berlijn, R. Fittipaldi, V. Granata, A. Vecchione, P. Wahl, and P. Hirschfeld, *npj Quantum Mater.* **6**, 100 (2021).
- [40] C. Xia, J. Wu, Y. Chen, and H. Chen, *Phys. Rev. B* **105**, 115134 (2022).
- [41] M. Kim, J. Kwon, C. H. Kim, Y. Kim, D. Chung, H. Ryu, J. Jung, B. S. Kim, D. Song, J. D. Denlinger *et al.*, *npj Quantum Mater.* **7**, 59 (2022).
- [42] R. Yu, J.-X. Zhu, and Q. Si, *Curr. Opin. Solid State Mater. Sci.* **17**, 65 (2013).
- [43] R. Yu and Q. Si, *Phys. Rev. B* **96**, 125110 (2017).
- [44] R. Fresard, Many-Body Physics: From Kondo to Hubbard Modeling and Simulation **5** (2015).